Fresenius Z Anal Chem (1989) 333:466–469

Fresenius Zeitschrift für
Analytische
Chemie

Depth profiles of $Ta_2O_5/SiO_2/Si$ structures: a combined X-ray photoemission, Auger electron, and secondary ion mass spectroscopic study

P. Gimmel, B. Gompf, D. Schmeißer, and W. Göpel

Institut für Physikalische und Theoretische Chemie, Auf der Morgenstelle 8, D-7400 Tübingen, Federal Republic of Germany

Tiefenprofile von $Ta_2O_3/SiO_2/Si$-Strukturen: Eine kombinierte Untersuchung mit Röntgen-Photoemissions-, Auger-Elektronen- und Sekundär-Ionen-Massen-Spektrometrie

Summary. We prepared thin films of tantalum oxide on SiO_2/Si substrates by thermal oxidation of tantalum. The different oxide layers and their interfaces were characterized by SIMS, AES, and XPS. Characteristic structures were obtained after different oxidation procedures. The comparative discussion of AES and SIMS depth profiles makes possible an unequivocal characterization of the reactive interfaces between the oxides of Ta and Si. The Ta_2O_5/SiO_2 interface in particular shows non-stoichiometries which depend on the oxidation procedures and which determine the performance characteristics of pH-sensitive Ta_2O_5 field-effect transistors.

1 Introduction

Tantalum pentoxide (Ta_2O_5) has various applications in semiconductor technology such as its use as capacitor material in VLSI-technology, as material for electrical resistors, as gate insulator for field-effect transistors (FET's), and as pH-sensitive layer for ion-sensitive FET's (ISFET's) [1, 2].

The latter was of primary interest for our studies. A schematic set-up of an ISFET is given in Fig. 1 to illustrate the importance of controlled interface structures and the importance of interface analysis in optimizing the performance of ISFET's. The liquid-solid interaction at the Ta_2O_5/electrolyte interface causes a potential variation that changes the potential at the gate electrode against a reference electrode, and in turn, changes the electrical characteristics of the ISFET. For the reliable electrical performance of an ISFET, its different gate oxides should have a homogeneous composition and the interfaces between these oxides should not be smeared out. Both requirements result in a low density of impurities and also in a low density of uncontrolled electrically active defects in the layer structures.

In this paper we describe first results from our experimental approach to combine thin film preparation of ISFET layer structures with their spectroscopic in-situ characterisation.

Offprint requests to: P. Gimmel

2 Experimental

In a first set of experiments (samples of type 1) we prepared Ta films under UHV conditions ($p < 10^{-7}$ Pa). We used p-doped silicon substrates with a 46 nm thick SiO_2 layer and prepared ultra-thin tantalum layers in the monolayer range by thermal evaporation from an electrically heated Ta-wire with a purity of 99.99%. The resulting films had thicknesses between 0.5 and 2.5 nm as monitored in XPS by applying Beer's law.

In a second set of experiments (samples of type 2) we prepared different Ta_2O_5 layers by thermal oxidation of e-gun evaporated tantalum films ($d_{Ta} = 53$ nm). The following oxidation process was done in a pure oxygen atmosphere (1 bar) at temperatures between 800 and 850 K. For different oxidation times we obtained partly ($t_{ox} = 10$ min) and fully ($t_{ox} = 20$ min) oxidized samples [3]. The resulting Ta_2O_5 is amorphous [4, 5]. Elemental composition and stoichiometry of the layers was controlled by AES and XPS [6–8]. During the spectroscopic measurements, samples were kept at room-temperature.

Auger depth profiles were done in a scanning Auger microscope (SAM) (Perkin Elmer PHI 600), with a typical primary electron current of 1 μA at 10 keV. Sputtering was performed with Ar^+ ions at 4 keV with a scanned ion beam (2×2 mm^2, 400 nA, 45°).

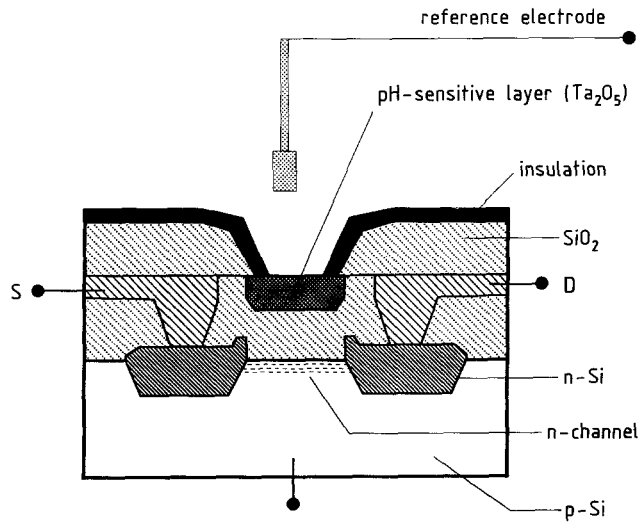

Fig. 1. Interfaces of an ion-sensitive field-effect transistor (ISFET) in a schematic drawing. The bias voltage at constant current between source (*S*) and drain (*D*) is used to monitor pH values

XPS and SIMS experiments were performed in a separate UHV combination system which allowed controlled heating of the sample up to 1500 K. By means of an UHV transfer vessel samples could be manipulated between the different spectrometers, sample preparation stages, a high pressure ($p \leqslant 30$ bar) reaction cell, and an electrochemical cell for ISFET characterization under controlled conditions [9]. The Ta evaporation and initial sample cleaning was performed in a preparation vessel by ion bombardment and annealing.

XPS spectra were obtained with a double anode set-up with AlK_α (1486.6 eV) and MgK_α (1253.6 eV) radiation.

SIMS depth profiles were recorded using a single-lens ion extraction optics and a quadrupole mass spectrometer (Balzers QMG 420). Beam scanning, gating, and data recording was computer controlled. All SIMS sputter profiles were taken with O_2^+ primary ions (ion source: Telefocus, Atomika) with an acceleration voltage of 10 keV ($1-2\times10^{-3}$ cm^2, 30 nA, 45°). To avoid crater wall effects, a 59% electronic gating was used. The use of a Wien filter eliminated impurities, neutral atoms, and doubly charged ions. For some of the SIMS profiles a flood-gun had to be used for charge compensation of highly insulating samples.

3 Results and discussion

3.1 XPS data (samples of type 1)

Figure 2 shows typical XPS spectra of the Ta 4f region after different tantalum evaporation and heating cycles as indicated in the figure. The binding energy is referred to the Fermi level. For comparison, the binding energy of the Ta 4f (7/2) peak recorded from a clean Ta foil is indicated by an arrow. All spectra are corrected for a slight charge-up (0.7 eV) of the sample.

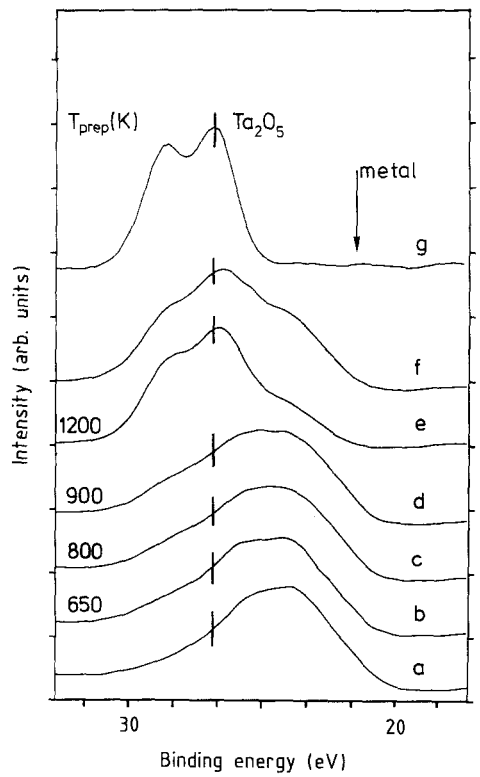

Fig. 2. XPS (MgK_α) spectra of the Ta 4f region: the first spectrum *a* was taken after evaporation of Ta on Si/SiO_2 substrates with $d_{Ta} = 0.5$ nm. *b–e* are obtained after annealing the sample to different preparation temperatures T_{prep}. Spectrum *f* is obtained after a subsequent additional Ta evaporation with $d_{Ta} = 0.7$ nm. *g* was obtained after a final oxidation procedure ($T = 800-850$ K, $p(O_2) = 1$ bar, $t = 75$ min)

After the first Ta evaporation cycle, the tantalum layer thickness on SiO_2 is determined to be 0.5 nm (Fig. 2a). With increasing annealing temperatures the curve maximum shifts towards higher binding energies (Fig. 2b–e). Figure 2f was recorded after further tantalum evaporation. Here, the layer thickness is increased to 0.7 nm. In Figure 2e and f, the maximum of the curve shifts to about 28 eV. Figure 2g shows the Ta 4f region after a final oxidation procedure for which the sample was kept at about 850 K with an oxygen pressure of 1 Pa for 75 min. The corresponding Ta 4f levels are shifted by 5 eV with respect to the metallic Ta peak [5–8, 10].

The shape of the curve observed after initial Ta evaporation with a peak maximum at about 25 eV indicates that there is no emission from metallic Ta, rather than from a mixture of Ta oxides with different oxidation states.

These XPS data indicate that Ta is oxidized under UHV conditions in an interaction with SiO_2 even at room temperature. From the shape of the Ta 4f emission the stoichiometry of the film can be determined.

3.2 Depth profiling with AES (samples of type 2)

Figures 3 and 4 show Auger depth profiles with the Auger intensity of a partly oxidized (Fig. 3) and of a fully oxidized sample (Fig. 4) plotted versus the sputter time. Depending on the oxidation conditions, the depth profiles can be separated into distinct or smeared out regions as shown in Figs. 3–6. Although the location of the different interfaces between the regions requires a tentative assignment, it is nevertheless a useful concept to distinguish between 5 different regions.

For both samples region 1 corresponds to stoichiometric Ta_2O_5, as it was verified by XPS. Region 2 represents a

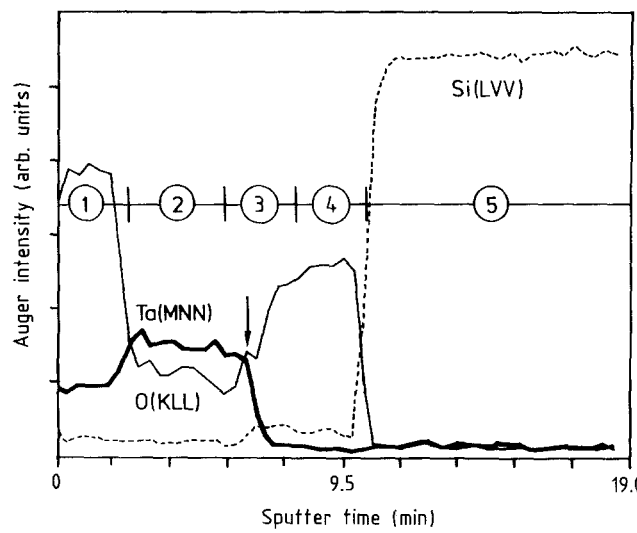

Fig. 3. AES profile of a partly oxidized Ta_2O_5 layer on SiO_2/Si. Region *1* characterizes a stoichiometric Ta_2O_5 layer at the surface (as e.g., verified with XPS). The region *2* is the partly oxidized layer. Region *3* indicates the Ta_2O_5/SiO_2 interface. Region *4* is the SiO_2 layer, and region *5* is the bulk silicon

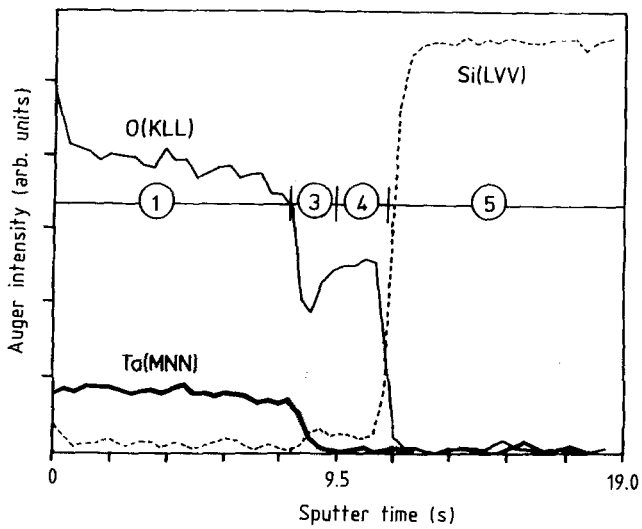

Fig. 4. AES profile of the fully oxidized sample. Region *2* (see Fig. 3) is not observed here, and region *3* is narrower than in Fig. 3

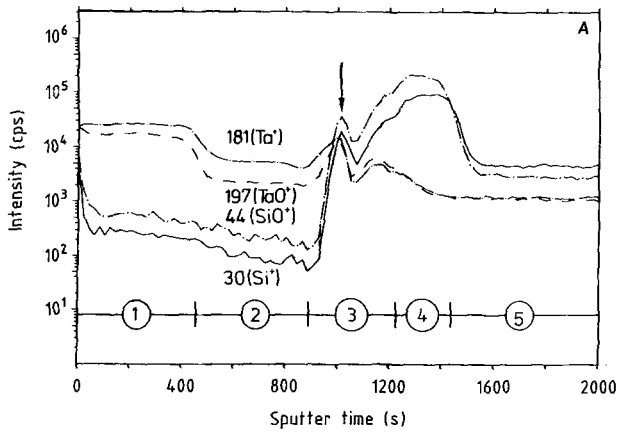

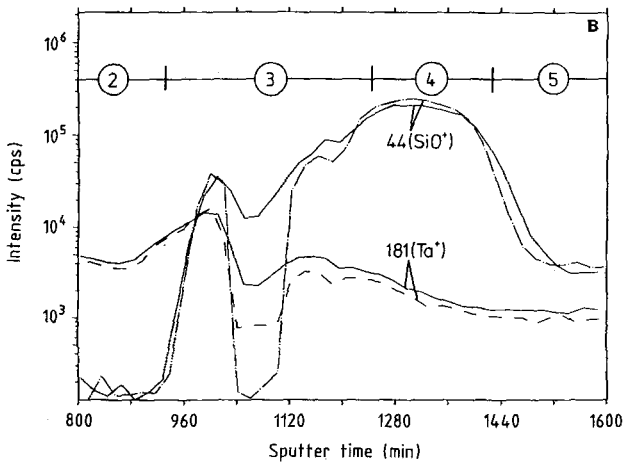

Fig. 5. **A** SIMS depth profile of the same sample as in Fig. 3 (flood-gun used). **B** SIMS depth profiles of the same sample as in **A**, with/without (*crushed lines*) use of a flood-gun

partly oxidized tantalum layer (Fig. 3 only) and characterizes a non-stoichiometric TaO_y ($y < 2.5$). Region 3 is the Ta oxide/SiO_2 interface. Region 4 is the initial SiO_2 layer with its SiO_2/Si interface towards the bulk Si in region 5.

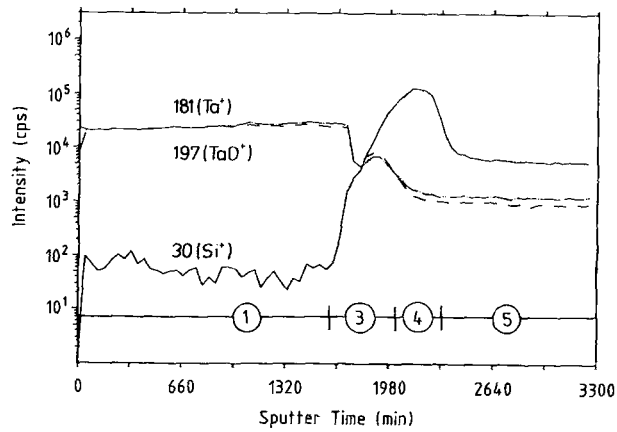

Fig. 6. SIMS depth profile of the same sample as in Fig. 4 (flood-gun used)

In the following we will concentrate on the Ta_2O_5/SiO_2 interface (region 3) since we expect drift effects in ISFET device performance partly to be caused by an enhanced defect concentration at this interface.

In partly oxidized samples (Fig. 3) a pronounced initial rise of the oxygen signal is always observed. This is indicated by an arrow in Fig. 3 and was verified for several depth profiles taken with varying ion beam currents at different spots of the same sample. The influence of different sputter conditions has been discussed in the literature [11–13]. In line with the XPS results (section 3.1), this discontinuity in the increase of the oxygen signal indicates different oxidation mechanisms of Ta at that interface and in the Ta layer.

In both samples the oxygen signal in region 4 raises continuously and does not reach a constant value as it would be expected for an ideal SiO_2 structure. In addition to matrix effects at the oxide/oxide interface, a slightly reduced oxygen concentration in the outer SiO_2 layer most probably determines that signal behavior.

3.3 Depth profiling with SIMS (samples of type 2)

The SIMS profiles may formally be separated in the same way as described above. Again, region 3 indicates the non-stoichiometric interface in Figs. 5 and 6.

The intensity increase (indicated by an arrow) in Fig. 5 of all masses in region 3 is due to a higher oxygen concentration and, hence, a higher ionisation probability as it may be deduced from the rise of the AES oxygen signal in Fig. 3 [14–17]. In accordance with our XPS results we deduce from this, that the tantalum located directly at the Ta/SiO_2 interface is not oxidized by the oxygen from the gas phase, but by oxygen originating from the SiO_2 layer itself. So a partly distored SiO_2 is produced and the increase of all signals in Fig. 5 characterizes a tantalum/silicon oxide mixture at this interface.

One reason for the following decrease of all intensities towards the SiO_2 layer is a charge-up effect at the oxide/oxide interface. Figure 5A shows region 3 of a partly oxidized sample in an extended scale. We show two depth profiles recorded with and without a charge neutralizing flood-gun. For simplification, masses m/e = 44, and m/e = 181 are plotted only. Obviously, the intensity decrease is influenced by the flood-gun. With charge compensation the minima of all masses are less pronounced. In accordance with the AES

profile in Fig. 3 the remaining decrease in signal intensity is attributed to a real oxygen deficiency in this interfacial region.

In the following we estimate the interface width by using erosion rates dz/dt from references samples, i.e., from Ta_2O_5/Ta and SiO_2/Si structures. Under the same sputter conditions as used to obtain the profiles in Figs. 5 and 6 we find $dz/dt = 0.069$ nm/s for Ta_2O_5 and $dz/dt = 0.12$ nm/s for SiO_2. In a first estimation of the width of region 3 we may either assume this section to have an erosion rate similar to SiO_2 or a value between SiO_2 and Ta_2O_5. The erosion rate of elementary silicon can be neglected because sputtering of Si with reactive O_2^+ ions is known to lead to sputtering rates similar to those of SiO_2 [14, 17–20]. With these assumptions we estimate an interface width of 16–27 nm for the poorly oxidized sample (Fig. 5) and of 12–21 nm for the fully oxidized sample (Fig. 6). It is clear that these values depend on the reliability of the above-mentioned assumptions and also on the definition of interfaces of the regions involved. This estimation does, however, show that the widths of these interfaces clearly extend the sputter-induced broadening and the spectrometer-dependent limitation of depth resolution [17–22].

An atomistic understanding of the reactive interface properties of the Ta/SiO_2 system may be obtained from thermodynamic considerations. Following those, Ta_2O_5 is less stable than SiO_2 under experimental conditions of our work. The formation of mixed Si/Ta oxides is thermodynamically unrealistic when Ta is evaporated onto SiO_2 [23–26]. In contrast to these facts, our XPS data of the samples of type 1 demonstrate the formation of mixed oxides if additional oxygen from the gas phase is excluded under UHV conditions. Here, reactions at the Ta/SiO_2 interface lead to defects in the SiO_2 layer and a partial oxidation of Ta which is linked with the chemical reduction of the SiO_2 lattice to form a non-stoichiometric SiO_x ($x < 2$) region. Even in the case of the samples of type 2, which were not prepared under UHV conditions, a broadened Ta oxide/Si oxide interface is indicated by our AES and SIMS depth profile results. Here the formation of this mixed oxide probably occurs in the early phases of the Ta oxidation procedure, and stops when a sufficient amount of oxygen from the gas phase reaches this interface.

Defects in oxygen-deficient SiO_2 are of great importance in silicon device technology, although no direct experimental access is available for their quantitative assignment. There are, however, several approaches that give evidence for their existence [27]. For the system investigated here, the existence of defects is evident from thermodynamic considerations and from deviations of the ideal stoichiometry at the SiO_2 interface as determined from XPS, AES, and SIMS data.

4 Conclusions and outlook

The results presented in this paper mainly deal with inhomogeneities occurring normal to the surface.

We found characteristic differences between partly and fully oxidized samples at the SiO_2/Ta_2O_5 interface. At the Ta oxide/SiO_2 interface both depth profiles indicate a pronounced inhomogeneous composition with respect to the oxides of Ta and Si.

We have demonstrated that comparative studies with AES, SIMS, and XPS including depth profiling lead to a detailed characterization of layer structures including mixed oxides. The information obtained in these studies is a prerequisite for understanding instabilities and for optimizing electronic devices such as ion-sensitive field-effect transistors with Ta_2O_5/SiO_2 gates [28].

Acknowledgements. We would like to thank W. Neu, B. Suhr, Th. Weitzel for technical assistance, and M. Klein (AEG Research Labs Ulm, FRG) for discussions and for supplying us some of the Ta_2O_5-samples. This work was supported by the BMFT, Fonds der chemischen Industrie, and Landesforschungsschwerpunkt Baden-Württemberg.

References

1. Janata J, Huber R (1985) Solid state chemical sensors. Academic Press, New York
2. Klein M, Kuisl M, Ricker T (1983) Tech Messen 50:381
3. Borisenko, VE, Parkhutik VP (1986) Phys Status Solidi (a) 93:123
4. Oehrlein GS, d'Heurle FM, Reisman A (1984) J Appl Phys 55:3715
5. Rossnagel SM, Sites JR (1984) J Vac Sci Technol A 2:376
6. Cros A, Tu KN, (1986) J Appl Phys 60:3323
7. Himpsel FJ, Morar JF, McFeely FR, Pollak RA, Hollinger G (1984) Phys. Rev. B30:7236
8. Bispinck H, Ganschow O, Wiedmann L, Benninghoven A (1979) Appl Phys 18:113
9. Göpel W Proc Eurosensors I, Cambridge 1987 and Sensors and Actuators, 1989, in press
10. Holloway PH, Nelson GC (1979) J Vac Technol 16:793
11. Zhe Q, Tian-Sheng X (1988) Surf Sci 194:L127
12. Petrakian JP, Renucci P (1988) Surf Sci 195:151
13. Hunt CP, Seah MP (1983) Surf Interface Anal 5:199; Seah MP, Holburn MW, Davies JA, Ortega C (1987) J Vac Sci Technol, A5:1988; Malherbe JB, Hofman S, Sanz JM (1986) Appl Surface Sci 27:355
14. Vandervorst W, Shepherd FR (1985) Appl Surf Sci 21:230
15. Wittmaack K, Wach W (1981) Nucl Instrum Methods 191:327
16. Vandervorst W, Maes HE, De Keersmaecker RF (1984) J Appl Phys 56:1425
17. Wittmaack K (1984) Vacuum 34:119
18. Benninghoven A, Rüdenauer FG, Werner FG (1987) Secondary ion mass spectrometry. Wiley, New York
19. Behrisch R (1981) Topics in applied physics. Sputtering by particle bombardement 1. Springer, Berlin Heidelberg New York
20. Behrisch R (1981) Topics in applied physics. Sputtering by particle bombardement 2. Springer, Berlin Heidelberg New York
21. Schwarz SA, Helms CR (1979) J Vac Sci Technol 16:781
22. Degreve F, Ged P (1983) Surf Interface Anal 5:83
23. Beyers R (1984) J Appl Phys 56:147
24. Searcy AW, Finnie LN (1962) J Am Ceram Soc 45:268
25. Fromm E, Kirchheim R (1975) Z Metallk 66:145
26. Chen JR, Liauh HR, Liu YC, Yeh FS (1983) J Vac Sci Technol A1:570
27. See, e.g., Schleich B, Schmeißer D, Göpel W (1987) Surf Sci 191:367, or Kunst M, Jaegermann W, Schmeißer D (1987) Appl Phys A 42:57, and references given there
28. Gimmel P, Gompf B, Klein M, Schmeißer D, Wiemhöfer HD, Göpel W (1988) Conf Proc of Eurosensors II, Twente, NL, and Sensors and Actuators, 1989, in press

Received November 15, 1988